ACS APPLIED NANO MATERIALS

www.acsanm.org Article

Methodology for the Computational Optimization of Nanoparticle Synthesis and Particle Size Distribution, Using $Ir(0)_n$ Nanoparticles as an Example System

Danny Long,* Richard G. Finke, and Wolfgang Bangerth

Cite This: *ACS Appl. Nano Mater.* 2024, 7, 14090–14101 Read Online

ACCESS | Metrics & More | Article Recommendations

ABSTRACT: Small particles at the nano- and micron-scale have found many applications made possible by their specific size, size distribution, and generally large surface-to-volume ratio. Yet, approaches to systematically designing these particles and their size distribution based on mechanistic principles—that is, being able to choose reaction conditions based on an established mechanism of formation—have so far largely eluded the field. Herein, we present a methodology that allows for optimizing reaction conditions in silico, using a well-characterized, prototype system of iridium nanoparticles as an example. We show that given a model of nanoparticle formation that we have previously vetted against experimental data, statistical estimates for the parameters in this model also previously obtained, and a suitable optimization algorithm, we can predict experimental conditions (such as initial concentrations and reaction end times) for which the resulting particle size distribution both closely matches a desired mean value, and is very narrow—that is, it allows for outcomes that enable many currently unattainable applications. Moreover, our methodology accomplishes this optimization task while also accounting for parameter uncertainty. The combination of model, parameter estimates, and optimization algorithm is generic and is applicable to many other nanoparticle systems as well, as long as a reliable model of the formation of these particles is available. Thus, we contribute a full analysis workflow where an understanding of kinetics equations is the only prerequisite mathematical knowledge.

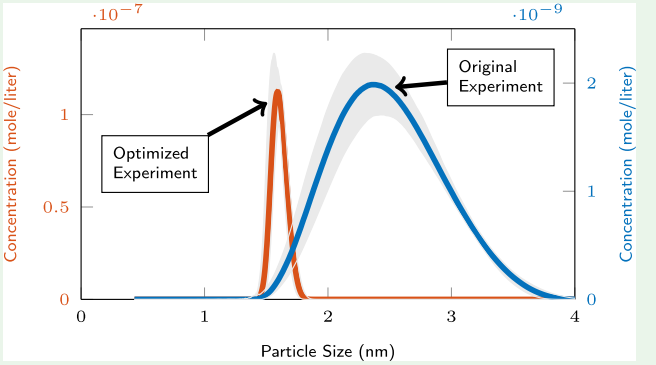

KEYWORDS: *nanoparticles, in silico optimization, synthetic control of particle size distribution, uncertainty quantification, population balance modeling*

1. INTRODUCTION

Nano- and micron-sized particles have found myriad applications over the past several decades.[1−9] Today, the syntheses of these particles are largely based on experience and trial-and-error[10] and often result in particles that have a wide range of sizes. Yet, because physical and chemical properties invariably depend on the particle size (PS) and particle size distribution (PSD), there is much to be gained if we can devise rational approaches to syntheses that produce particles of specific sizes and size distributions.

There are many practically important reasons for controlling the average PS and/or PSD since the physical properties of particles across materials chemistry, science, and indeed nature are invariably dependent on the average PS and width of the PSD. For example, for catalytic particles, such as the $Ir(0)_n$ particle system exploited herein, reactivity and selectivity (so-called "structure sensitivity"[11,12]) are size dependent; similarly, for semiconductor particles such as $(CdSe)_m$ and $(InP)_m$, size determines their color and thereby possible applications in electronics;[13−16] there are many other examples of particles with size- and PSD-dependent properties.[17−27]

As a consequence of such considerations, one of the grand challenges of working with nano- and micron-sized particles is the development of a rational, predictive approach toward the synthesis of particles with specific sizes or size distributions. Herein, we describe a methodology for computational optimization of PSs and size distributions that is based on a mathematical model of nucleation and formation of iridium nanoparticles. It utilizes the computational power available today to replace the traditional (educated) trial-and-error

Received: March 6, 2024
Revised: May 21, 2024
Accepted: June 4, 2024
Published: June 17, 2024

https://doi.org/10.1021/acsanm.4c01373
ACS Appl. Nano Mater. 2024, 7, 14090−14101

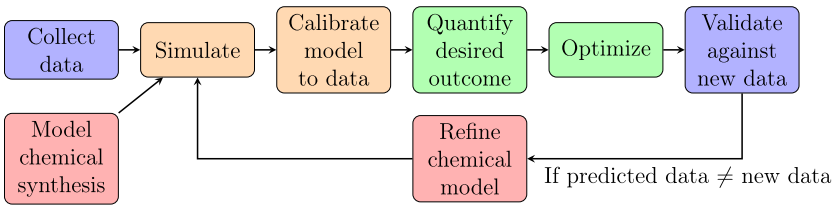

Figure 1. A flowchart illustrating our analysis, modeling, and optimization pipeline. Blue: experiments; red: mathematical modeling of the chemical system; yellow: computational and statistical aspects of modeling; green: optimizing synthesis conditions. This contribution addresses the green rectangles, whereas our previous work has addressed the others.

approach with a systematic exploration of parameter space, based on the workflow shown in Figure 1.

Concretely, we present predictive control of PS and PSD based on a model for the growth of iridium nanoparticles that we have previously validated using experimental data.[28−30] The specific model we consider resulted from comparing many possible models for the formation of $Ir(0)_n$ nanoparticles, all rooted in mechanistic insight into the nucleation and growth process (we call such models "mechanism-enabled (ME)"), and ruling out those that were not able to describe experimental observations; all candidate models we considered track the concentrations of each size of nanoparticles separately (we thus use the term "population balance" to indicate that we model population numbers via balance equations). As a consequence, the model we use for our optimization studies falls into the category of "ME population balance models (ME-PBM)" that are able to make very specific predictions not only for size statistics such as the average PS but indeed for the entire PSD.[28−31]

While we focus on the ME-PBM class of models in this contribution, we note that this is not a restriction; any other accurate model able to predict the number of particles of specific sizes (i.e., the PSD) would do as well. Indeed, our optimization approach only requires some function that maps experimental conditions to a PSD. Hence, other modeling approaches such as the method of moments,[32] the quadrature method of moments,[33,34] and the exact method of moments[35] fit equally well into our optimization framework. All of these variations of the method of moments track the statistical moments of the PSD (e.g., the first moment is the mean value, and the second moment is the standard deviation) instead of tracking the number or concentration of particles of all possible sizes. By using such a reduced description of the PSD, these methods greatly decrease the computational cost of predicting a PSD compared to the population balance model we present in Section 2. However, appropriately connecting the method of moments with the chemical reactions occurring in synthesis is difficult and substantially more mathematically complex than our method. Therefore, we omit further discussion of the method of moments but suggest the review in ref 34 as an introduction to this modeling methodology.

Ultimately, whether predictive control of PS and PSD is possible comes down to the question of whether the system (represented by our model) is sensitive to those parameters one can adjust in experimental settings. Herein, we demonstrate that we can control both the average PS and the PSD to desired values by adjusting the initial concentrations of the synthesis, how long the reaction is carried out, and—to obtain even better results—adjustment of reaction rates that we think can be achieved through means such as control of temperature, solvent, and other variables such as the particle-capping ligands employed. Excitingly, by demonstrating that the system in question allows for such optimized, predictive control puts within reach for the first time a rational approach toward the synthesis of iridium and other such nanoparticles and makes it credible that similar approaches can also be used for other widely used nanoparticle systems.

To the best of our knowledge, the work in ref 36 is the only other detailed, mathematical approach in the literature addressing the experimental design of nanoparticle systems to achieve a desired outcome. The approach outlined in ref 36 requires substantial mathematical sophistication and assumptions on the synthesis process (e.g., no agglomeration is taken into account). The result there is a clever formulation of the problem which can then be solved efficiently. The challenge with this approach, however, is that the typical experimentalist in the nanoparticle community does not have the expertise in their group required to perform this complex of a mathematical analysis. Our approach differs in that we allow for arbitrary reaction dynamics and limit the mathematical expertise required to that of formulating differential equations from systems of chemical reactions. This approach matches the level of mathematical expertise in the nanoparticle community; more importantly, it is applicable to a far wider range of systems than the sophisticated approach of ref 36.

The basis for our methodology is (i) the development of a mechanism-based model that accurately describes the growth of $Ir(0)_n$ nanoparticles upon which our study is based (which we provided in refs 28 and 29), (ii) an approach to use available experimental data to obtain statistical estimates of the parameters of the model such as reaction rates, including their best-fit values and error bars along with higher order moments (which we provided in refs 30 and 31), and (iii) an optimization method that systematically varies input experimental conditions to obtain desired outputs while accounting for the uncertainty in model parameters; that is, we perform optimization under uncertainty. It is this last point that is the focus of this paper: we will provide a computational approach to optimization, and demonstrate that this approach results in outcomes close to desired values for PSs or PSDs. As mentioned above, the methodology we present uses the iridium system as a test case, but it does not rely on the specifics of the model. Indeed, we stress that the contribution of this paper is the methodology, not its application to a specific nanoparticle system.

Concisely, we herein address the following questions, all in the affirmative:

1. Can we formulate a simulation-based methodology that optimizes experimental outcomes to match prechosen PS and PSD, often focused on as narrow a PSD as possible and considering simulation uncertainty?
2. Can we provide an optimization strategy (and associated software implementation) using an algorithm that

https://doi.org/10.1021/acsanm.4c01373
ACS Appl. Nano Mater. 2024, 7, 14090−14101

researchers who are not experts in mathematics or the computational sciences can understand and readily use?

3. Can we then actually obtain optimization results for a known, prototype nanoparticle-formation system as proof of principle?

These questions address how one would approach the blue boxes in Figure 1 given that these steps by themselves represent a gap in the available literature. Ultimately, of course, one would like to close the workflow (as shown in the figure) into an iterative process that includes experimental validation of computational predictions, as well as refinement of the mathematical model of nanoparticle synthesis. While we would of course have liked to "close the loop" herein as well, we will have to leave this to future work: the experimental realization of the system is outside the range of what the authors' laboratories can perform these days.

Herein, we introduce the mathematical framework necessary for our approach in Section 2. This framework includes a brief discussion of ME-PBM, a presentation of the ordinary differential equation (ODE) model that arises from ME-PBM, and the results of the Bayesian inverse problem to characterize unknown model parameters and their uncertainty. Next, in Section 3 we describe our formulation of an "optimal" PSD, how one can compute this quantity, and the algorithm we employ to find the optimal experimental conditions. Finally, in Section 4 we present numerical results of our optimization procedure and our associated discussion thereof. We conclude in Section 5.

2. MATHEMATICAL MODEL FOR IR(0)$_N$ NANOPARTICLE FORMATION

Computational optimization requires a mathematical model whose inputs can be systematically altered to observe how its outputs compare against an objective function that encodes desired outcomes. For this work, we will use a model for the nucleation and growth of Ir(0)$_n$ nanoparticles for which we have spent years developing appropriate reaction conditions,[37] experimentally characterizing reaction outcomes,[38] deriving mathematical models,[28,29] and statistically determining reaction rates and other parameters of the model by comparing model outcomes against experimental data.[30,31] Notably, we have also spent a large amount of work on rejecting many alternative ideas for how nucleation and growth could proceed (and therefore falsified the hypothesis that any of the corresponding models could be correct because we could show that these models could not fit the data), along with rejecting some models that did fit the data but were unnecessarily complicated compared to the simplest models that fit the data. We refer the reader to ref 29 for details on this prior work.

In the following, let us therefore give a brief overview of the system under consideration, along with the model we will use, and the reaction rates we have inferred by calibrating against experimental data. That said, we want to stress that everything we say about optimizing the outcomes of this model is expected to also hold for other nanoparticle and larger systems; we simply choose the Ir(0)$_n$ system investigated herein because it is a prototype system where all the necessary building blocks are available to demonstrate model optimization.

2.1. Synthesis of Ir(0)$_n$ Nanoparticles. The Ir(0)$_n$ particles and associated PSDs were prepared using the reactionstarting with $\{(1, 5{-}\mathrm{COD})\mathrm{Ir}^{\mathrm{I}}\cdot\mathrm{POM}\}^{8-}$ then placing the system under H_2 as detailed in ref 39 and the references therein. Transmission-electron microscopy (TEM) micro-

$$\sim 300[(1,5{-}\mathrm{COD})\mathrm{Ir}\cdot \mathrm{P_2W_{15}Nb_3O_{62}}]^{8-} + 750\,\mathrm{H_2} \longrightarrow \mathrm{Ir(0)}_{\sim 300} + \sim 300\,\bigcirc + \sim 300\,[\mathrm{P_2W_{15}Nb_3O_{62}}]^{9-} + 300\,\mathrm{H^+}, \quad (1)$$

graphs of the Ir(0)$_n$ nanoparticle product were obtained at Clemson University.[39] Conditions for the TEM sample preparations were 1.2 mmol $\{(1, 5{-}\mathrm{COD})\mathrm{Ir}^{\mathrm{I}}\cdot\mathrm{POM}\}^{8-}$ in acetone.[39] The PSDs were created by measuring and organizing the PSs into bins at ±0.05 nm intervals (i.e., 0.1 nm total; 0.85−0.94 nm were considered to be 0.9 nm, 0.95—1.04 were considered to be 1.0 nm, etc.). Four distributions were collected at 0.918, 1.170, 2.336, and 4.838 h (the original times measured in seconds, then converted to hours and the correct number of significant figures indicated), with 246, 61, 150, and 213 particles measured, respectively. The mean sizes and standard deviations are, respectively, 2.0 ± 0.4, 2.4 ± 0.6, 2.5 ± 0.4, and 2.8 ± 0.4 nm. The PSD data were then analyzed by ME Population Balance Modeling as detailed in our 2019 and 2020 publications.[28,29]

2.2. Conceptual Model in Pseudoelementary Steps. Our mathematical models for the nucleation and growth of Ir(0)$_n$ nanoparticles are based on "pseudo-elementary" reactions[40] between the original molecular reagents and "classes" of particles (such as "small" and "large" nanoparticles). The steps we choose are informed by experimental kinetics and a mechanistic understanding of the chemical reactions that take place and are therefore "ME", using the terminology outlined in the introduction.

In translating these conceptual models of pseudoelementary steps into concrete, ODEs, we use a population balance approach. In other words, we break each class of particles into concentrations of particles of specific sizes (indexed by the number of iridium atoms in a particle). The concentrations of particles of each size (the "populations") evolve based on balance relationships that fundamentally encode mass conservation; the models are therefore called PBM. In this subsection, let us discuss the classes of particles we consider, along with the pseudoelementary steps; we will then discuss the translation into an ODE model in Sub-section 2.3.

The model we will use herein is based on our findings in ref 29, and in keeping with the notation from this reference, we will refer to it as the "3-step mechanism," even though the first nucleation process is composed of two steps, steps 0 and 1 below. This mechanism includes the following steps:

0. The dissociation of a ligand-bound precursor into the precursor itself (in solution) and the ligand;
1. A continuous nucleation mechanism creating the smallest nanoparticles containing just three iridium atoms from a precursor;
2. Small particles grow quickly by reaction with the precursor species;
3. Large particles grow slower by reaction with the precursor species.

The slowing down of the reaction rate between small and large particles allows smaller particles to catch up in size with larger particles, leading to the observed narrow distribution of PSs at the end of the reaction, despite the fact that small particles are continuously created.[29]

The 3-step mechanism, using the notation used in previous work,[29] can be expressed in the following form where A is the precursor, L is the ligand, B indicates the class of "small particles" and C is the class of "large" ones

https://doi.org/10.1021/acsanm.4c01373
ACS Appl. Nano Mater. 2024, 7, 14090−14101

$$
\begin{aligned}
&2\{\{\mathrm{A{\cdot}L} + 2\,\mathrm{solv} \underset{k_b}{\overset{k_f}{\rightleftharpoons}} \mathrm{A(solv)_2} + \mathrm{L}\},\\
&2\mathrm{A(solv)_2} + \mathrm{A{\cdot}L} \overset{k_1}{\rightarrow} \mathrm{B_3} + \mathrm{L} + 4\,\mathrm{solv},\\
&\mathrm{A{\cdot}L} + \mathrm{B} \overset{k_2}{\rightarrow} \mathrm{C} + \mathrm{L},\\
&\mathrm{A{\cdot}L} + \mathrm{C} \overset{k_3}{\rightarrow} 1.5\mathrm{C} + \mathrm{L}
\end{aligned} \tag{2}
$$

Important to note here is the 12 alternative mechanisms we considered in arriving at the 3-step mechanism above, but that all alternatives were either unable to predict the observed PSD or were more complex yet did not lead to better fits than the 3-step mechanism above.[29] As a consequence, the 3-step mechanism is—according to our evidence—the smallest mechanism compatible with the data, and we will, therefore, use the 3-step mechanism as the basis for our optimization work which follows.

2.3. Translation into an ODE Model. The ME-PBM framework involves translating the mechanistic reaction 2 to a system of ODEs through the law of mass action. These ODEs track the concentrations of each chemical species over time. The chemical species include the precursor, ligand, and associated molecules created during the nucleation reactions, as well as particles of each tracked size—that is, particles containing three iridium atoms, four iridium atoms, etc.[29−31] Denoting by $A_L = A_L(t)$ the concentration of precursor molecules bound to ligands, $A_s = A_s(t)$ the concentration of solvated precursor, $L = L(t)$ the concentration of ligands, and $P_i = P_i(t)$ for $i = 3, ..., J$ the concentration of nanoparticles with i iridium atoms (encompassing both the "small" and "large" class of particles), this system then reads as follows

$$
\begin{aligned}
\frac{\mathrm{d}A_L}{\mathrm{d}t} &= \underbrace{-k_f A_L S^2 + k_b A_s L - k_1 A_L A_s^2}_{\text{nucleation}} \underbrace{- A_L \sum_{j=3}^{J} \beta_j P_j}_{\text{growth}},\\
\frac{\mathrm{d}A_s}{\mathrm{d}t} &= \underbrace{k_f A_L S^2 - k_b A_s L - 2k_1 A_L A_s^2}_{\text{nucleation}},\\
\frac{\mathrm{d}L}{\mathrm{d}t} &= \underbrace{k_f A_L S^2 - k_b A_s L}_{\text{nucleation}} + \underbrace{A_L \sum_{j=3}^{J} \beta_j P_j}_{\text{growth}},\\
\frac{\mathrm{d}P_3}{\mathrm{d}t} &= \underbrace{k_1 A_L A_s^2}_{\text{nucleation}} - \underbrace{\beta_3 A_L P_3}_{\text{growth}},\\
\frac{\mathrm{d}P_i}{\mathrm{d}t} &= \underbrace{A_L(\beta_{i-1} P_{i-1} - \beta_i P_i)}_{\text{growth}}, \qquad 4 \le i \le J.
\end{aligned} \tag{3}
$$

Since nucleation creates particles with three iridium atoms, this system of equations starts tracking the concentration of particles of size i with P_3. We only consider particles up to size $J = 2500$; this is as a sufficiently large upper bound based on the fact that our data does not contain particles exceeding 4 nm, along with an empirical relationship between particle diameter and number of atoms in a particle.[29]

The eq 3 contains reaction rate parameters β_j that are related to the chemical rate constants k_2, k_3 in (2). We account for the physical fact that growth by monomer addition occurs on the particle's surface; hence, we make the assumption that the actual reaction rate of particle growth is proportional to the number of surface atoms a particle has. The fraction of surface atoms relative to the total number of atoms can be approximated as $r_i = 2.677 i^{-0.28}$, see ref 41, and hence the total number of surface atoms for a particle containing i total atoms is

$$
\alpha_i = i r_i \tag{4}
$$

If we further consider M to be a parameter describing the cutoff between small and large particles, then we can succinctly express the reaction rate of particle growth for the specific reaction

$$
\mathrm{A{\cdot}L} + \mathrm{B}_i \overset{\beta_i}{\rightarrow} \mathrm{B}_{i+1} + \mathrm{L}
$$

by

$$
\beta_i = \begin{cases} k_2 \alpha_i, & 3 \le i \le M, \\ k_3 \alpha_i, & M < i \le J \end{cases} \tag{5}
$$

which is the parameter used in (3).

The model above is then augmented by initial conditions for each concentration

$$
\begin{aligned}
A_L(t=0) &= A_0,\\
A_s(t=0) &= 0,\\
L(t=0) &= \mathrm{POM}_0,\\
P_i(t=0) &= 0, \qquad 3 \le i \le J,
\end{aligned} \tag{6}
$$

where all concentrations have units mol L^{-1}, and where POM indicates polyoxometalate (the specific ligand used in the experiments that spawned our work, see ref 29). The experimental design from which our data are collected corresponds to $A_0 = 1.2 \times 10^{-3}$ and $\mathrm{POM}_0 = 0$. Hence, the parameter estimates used herein, as shown in Table 1 and Figure 2, originate from these initial concentrations. At the same time, in the optimization strategy our work uses, we allow for the initial concentrations of A_L and L to vary within a wide range of feasible concentrations; see Section 3.1 for more details.

Table 1. Statistical Estimates for the Reaction Rate and Size Cutoff Parameters in the Model (3), as Inferred From Experimental Data in ref 39[a]

parameter	MAP	mean	2.5−97.5% quantile
k_f	1.2×10^{-3}	1.2×10^{-3}	$(1.1-1.4) \times 10^{-3}$
k_b	7.4×10^{3}	7.5×10^{3}	$(6.6-8.5) \times 10^{3}$
k_1	5.5×10^{5}	5.7×10^{5}	$(4.4-7.0) \times 10^{5}$
k_2	20.3×10^{5}	19.5×10^{5}	$(8.2-31.4) \times 10^{5}$
k_3	5.5×10^{3}	5.6×10^{3}	$(5.4-5.8) \times 10^{3}$
M	110	108	102−114

[a]Using Bayesian inversion. MAP is the "maximum a posteriori" (most likely) value for each parameter. Mean and two-sigma values are also provided. The posterior distribution for each parameter is visualized in Figure 2.

In summary, (3−6) provides an ODE model that can be used to predict the concentration $P_i(t)$ of particles with i iridium atoms—that is, the PSD. The model contains a number of parameters that are summarized in Table 2. In previous work, we have performed extensive parameter estimation studies based on experimental data, determining not only best-fit values for each parameter but statistical distributions that a particular parameter value is correct, using a Bayesian inversion approach;[30,31,42] we summarize key statistics for these parameters in Table 1 and

https://doi.org/10.1021/acsanm.4c01373
ACS Appl. Nano Mater. 2024, 7, 14090−14101

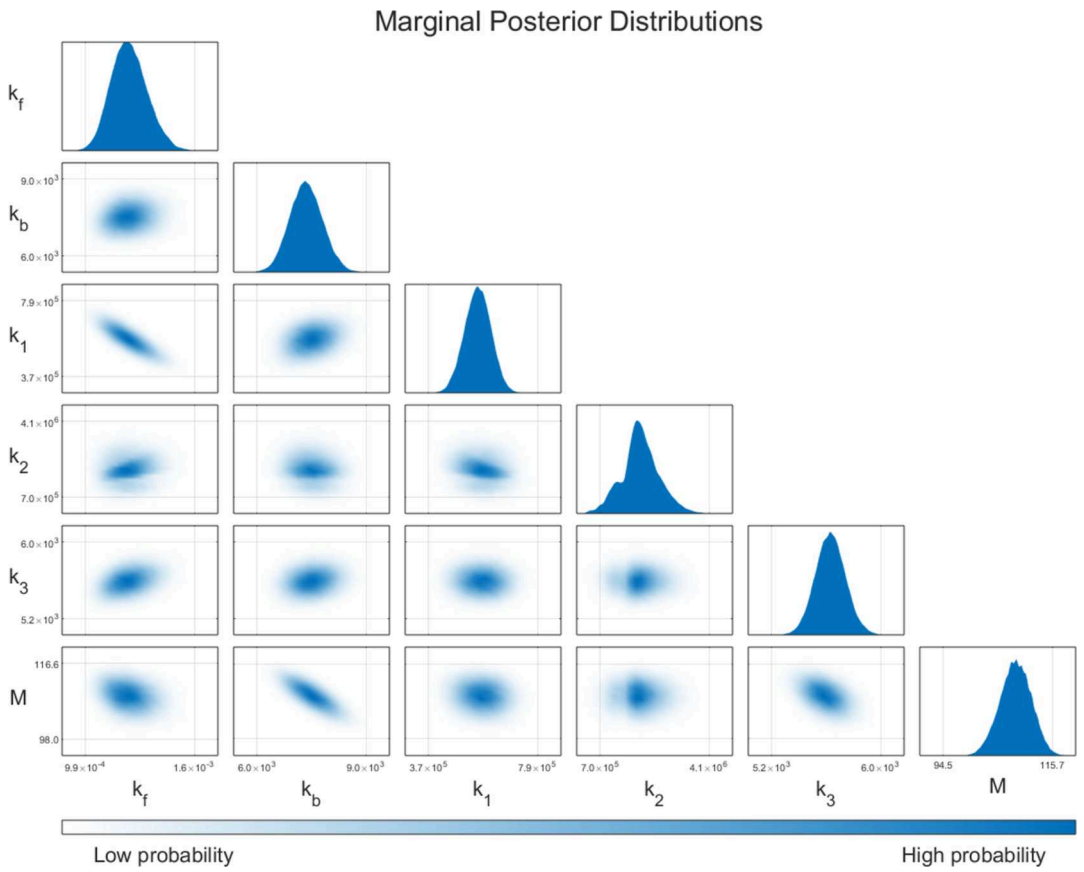

Figure 2. Probability maps in the form of one- and two-dimensional marginal distributions of the parameters in the 3-step mechanism after performing Bayesian inversion[30,31] The diagonal shows the one-dimensional marginals, that is, the probability that a given parameter value is correct. The lower-triangular regions show the two-dimensional marginals as indicated by the row and column labels; these plots therefore show the correlation between estimates for these parameters as inferred from the experimental data used in the Bayesian inversion.[30,31] Summary statistics for all of these parameters are also shown in Table 1.

Table 2. List of all Parameters in the ODE Model (3−6), Along with Their Meaning and Physical Units[a]

parameter	description	units
k_f	forward reaction rate in (2)	$L^2\ mol^{-2}\ h^{-1}$
k_b	backward reaction rate in (2)	$L\ mol^{-1}\ h^{-1}$
k_1	nucleation reaction rate in (2)	$L^2\ mol^{-2}\ h^{-1}$
k_2	small particle growth reaction rate	$L\ mol^{-1}\ h^{-1}$
k_3	large particle growth reaction rate	$L\ mol^{-1}\ h^{-1}$
M	cut-off size between small and large particles	unitless
t_{end}	end time of the reaction	h
A_0	initial precursor concentration	$mol\ L^{-1}$
POM_0	initial POM concentration	$mol\ L^{-1}$

[a]The first group of parameters, above the horizontal line, corresponds to the properties of the reaction; the second group are properties of the experimental setup.

show probability maps in Figure 2. We refer readers unfamiliar with Bayesian inverse problems to ref 43 for a simple introduction to the Markov Chain Monte Carlo (MCMC) approach used to solve these problems, along with some software packages with implementations of practical MCMC algorithms.[44−47]

3. OPTIMIZATION METHODOLOGY

The goal of this study is to explore whether we can use the model of the previous section to optimize the results of the reaction described. More concretely, guided by many practical applications (current and future), we want to see whether we can select reaction conditions so that specific nanoPSDs result.

In this and the following section, let us demonstrate that it is indeed possible to optimize the PSD predicted by the model introduced in the previous section. In other words, this section does not only demonstrate that the PSD is *sensitive* to experimentally accessible variables such as reactant concentrations and the time at which we terminate the reaction, but also that the sensitivity is sufficiently broad that we can achieve practically interesting PSDs.

Computational optimization of chemical reactions is a well-studied subject and we point the reader to a recent review for an overview of the field.[48] Moreover, the optimization algorithm we employ—Bayesian optimization—has started to gain traction in chemistry optimization problems in recent years.[49−52] However, accounting for uncertainty remains an understudied topic in the nanoparticle community. Experimental data have uncertainty and mathematical models for the kinetics of nanoparticle syntheses also have uncertainty, so consideration of these statistical distributions must be taken to robustly perform simulations. We demonstrated how to quantify this uncertainty during parameter estimation in ref 30. Now, the novelty of our current work is to retain and incorporate this uncertainty quantification during the optimization process of nanoparticle synthesis. That is, we now show how one can use quantified uncertainty in a productive and practical manner.

https://doi.org/10.1021/acsanm.4c01373
ACS Appl. Nano Mater. 2024, 7, 14090−14101

In the following, let us first introduce the variables we consider for variation (Section 3.1). We will then describe how we formulate the objective function, that is the "goal" of the optimization (Sections 3.2 and 3.3), and finally introduce an algorithm that finds this optimum (Section 3.4). We will discuss the results of this algorithm in the following Section 4.

3.1. Experimental Variables. The model described in Section 2.3 has a number of parameters (summarized in Table 2) that can roughly be subdivided into ones that are specific to the reaction (reaction rates, the size cutoff between small and large particles) and ones that are specific to the experimental conditions (end time of the reaction, initial conditions). For the former set of parameters, we have obtained estimates for the physically correct values via a Bayesian inversion approach,[31] as shown in Table 1, whereas the latter set corresponds to the parameter values chosen in the experiment whose measurements we had used for the parameter estimation procedure.

If one were to experimentally optimize the nanoPSDs, the obvious set of variables that are amenable to adjustment are the ones in the second category. Specifically, these are

- t_{end}: the time at which the reaction is stopped;
- A_0: the initial precursor concentration;
- POM_0: the initial POM ligand concentration.

In the following, we will group these three parameters under the name "experimental conditions". We will show the results of optimizing these parameters in Section 4.1.

On the other hand, the first group of parameters (namely, k_f, k_b, k_1, k_2, k_3, and M) is specific to the reaction at hand, and so not immediately accessible to systematic manipulation: They are what they are for a given experimental setup (characterized, for example, by the reaction temperature). That said, we will in Section 4.2 also investigate what happens if we could also make (some of) these parameters available for manipulation, and specifically if that allows us to further improve the desired outcomes of the reactions modeled by our system of ODEs. We note that adjusting these reaction parameters is often possible, for example by using the fact that reaction rates are a function of the temperature; it is also reasonable to assume that at least some of the reaction rates can be affected by choosing different ligands binding to the precursor, or other chemical modifications such as the presence of acids or bases.

In practice, it will likely be difficult to choose all reaction rates independently. Rather, in the experiments shown in Section 4.2, we will assume that we have control over the following specific factors:

- α_{kf}: A multiplier to the k_f reaction rate. Implementing a specific value for this factor could be achieved by diluting the solvent ($\alpha_{kf} < 1$), using a different solvent that acts as a stronger competing ligand ($\alpha_{kf} > 1$), or changing the ligand from POM to one of a range of other known nanoparticle stabilizers;[53]
- α_{k1}: A multiplier to the k_1 reaction rate. Implementing a specific value for this factor could be done by adjusting the temperature the reaction is conducted at, the solvent used to coordinate to the precursor, the particle-capping ligands, or other experimental factors. We do not currently know the temperature and other dependencies of these reaction rates nor the correlations between changes in k_1 to other reaction rates such as k_2 and k_3, but for the purposes of this proof-of-concept paper, we limit our study to modifying just k_1, while noting that it is precursor conversion and nucleation (k_1) that starts off the reaction and thus one expects k_1 to have a significant effect of the number of particles, initial reaction rate, and so on.

Below we will refer to α_{kf} and α_{k1} as "reaction factors" and will show the results of optimizing particle sizes by changing these parameters in Section 4.2. We summarize all the experimental conditions and reaction factors which we optimize over in Table 3, along with the intervals within which we allow these variables to range.

Table 3. List of all Experimental Variables Used to Optimize the PSD Along with the Bounds We Constrain the Variables to be between

variable	lower bound	upper bound
t_{end}	0.1 h	100 h
A_0	1×10^{-4} mol L^{-1}	1 mol L^{-1}
POM_0	1×10^{-4} mol L^{-1}	1 mol L^{-1}
α_{kf}	0.1	10
α_{k1}	0.1	10

3.2. Defining an "Optimal" PSD when Reaction Parameters are Known. Optimization requires the definition of an "objective function" that measures the quality of a predicted outcome of choosing specific inputs. In practice, we typically choose this function so that its minimum corresponds to the optimal outcome. In the following, let us denote by θ those variables we optimize over (i.e., either the experimental conditions, or the experimental conditions plus the reaction factors of the previous subsection), and by $\mathcal{K} = \{k_f, k_b, k_1, k_2, k_3, M\}$ the reaction rates and size cutoff parameter. Given a concrete set of values for θ and $\mathcal{K}$, we can then use the model of Section 2, (3−6), to predict a PSD $P_i(t_{end}; \theta, \mathcal{K})$, $i = 3, ..., J$, at the end time. Recall that $P_i(t; \theta, \mathcal{K})$ is the concentration of particles composed of exactly i iridium atoms.

Herein, we seek to determine the inputs that result in an optimal PSD. There are a variety of ways in which one can define what it means for a PSD to be "optimal", but most of them will include one or both of the following measures:

The mean PS

$$(\theta, \mathcal{K}) = \frac{\sum_{i=3}^{2500} P_i(t_{end}; \theta, \mathcal{K})\text{diameter}(i)}{\sum_{i=3}^{2500} P_i(t_{end}; \theta, \mathcal{K})} \tag{7}$$

Here, diameter (i) is a function that relates a number of atoms in a particle to its diameter in nanometers (see ref 29. The quantity $\mu(\theta, \mathcal{K})$ is appropriate to optimize in applications in which the specific size of nanoparticles is important—say, because of their optical properties that are strongly dependent on the size of particles.[5−8]

The standard deviation of the PSD

$$\sigma(\theta, \mathcal{K}) = \sqrt{\frac{\sum_{i=3}^{2500} P_i(t_{end}; \theta, \mathcal{K})[\text{diameter}(i) - \mu(\theta, \mathcal{K})]^2}{\sum_{i=3}^{2500} P_i(t_{end}; \theta, \mathcal{K})}} \tag{8}$$

This quantity is appropriate to minimize in applications in which it is important to have particles with a narrow size range, or in the extreme case, monodisperse particles.

https://doi.org/10.1021/acsanm.4c01373
ACS Appl. Nano Mater. 2024, 7, 14090−14101

In practice, one often wants both: particles should all have a very specific size, that is, one wants a specific value for $\mu(\theta; \mathcal{K})$, and one typically also wants a small value for $\sigma(\theta; \mathcal{K})$.

Finally, it would be wasteful for the reaction to not run to completion. Therefore, we also consider the conversion inefficiency

$$I_{\text{conversion}}(\theta, \mathcal{K}) = \frac{A_L(t_{\text{end}}; \theta, \mathcal{K})}{A_0(\theta)} \tag{9}$$

where $A_L(t_{\text{end}}; \theta, \mathcal{K})$ is the precursor concentration when the reaction is stopped at t_{end} and $A_0(\theta)$ is the initial precursor concentration. Since the set of optimization variables θ always includes A_0, $A_0(\theta)$ is simply one of the components of θ. Note that ideally $I_{\text{conversion}} = 0$, implying that all initially present material has been used up in the reaction, and that smaller values of $I_{\text{conversion}}$ are better (in keeping with our goal of minimizing the objective function).

Given these three goals, the objective (or "cost") function we would then like to optimize is of the form

$$C_{\text{deterministic}}(\theta, \mathcal{K}) = w_1|\mu(\theta, \mathcal{K}) - \hat{\mu}| + w_2\sigma(\theta, \mathcal{K}) + w_3 I_{\text{conversion}}(\theta, \mathcal{K}) \tag{10}$$

Here, $\hat{\mu}$ is the desired mean PS, and w_1, w_2, and w_3 are factors that allow us to weigh how much we care about each of the three goals mentioned above. We will choose these weights heuristically below. The subscript on $C_{\text{deterministic}}$ refers to the fact that we here assume that $\mathcal{K}$ is a known value, an assumption we will loosen in the next subsection.

In this framework, where we know the reaction rates encoded by $\mathcal{K}$ from a prior fit to data, the goal is then to find that set of control variables $\theta^*_{\text{deterministic}}$ that minimizes $C(\theta, \mathcal{K})$. In other words, we seek to solve the following deterministic problem: Find $\theta^*_{\text{deterministic}}$ so that

$$\theta^*_{\text{deterministic}} = \arg\min_{\theta} C_{\text{deterministic}}(\theta, \mathcal{K}) \tag{11}$$

3.3. Optimization under Uncertainty. As mentioned at the end of Section 2.3, we not only know the best-fit values for the parameters $\mathcal{K}$ by comparing them with experimental data, we also previously performed a Bayesian inversion that means we know the probability distribution $\pi(\mathcal{K})$ that describes how likely certain parameter values $\mathcal{K}$ are. Certain aspects of this probability distribution $\pi(\mathcal{K})$ are illustrated in Table 1 and Figure 2 where we show statistical estimates and marginal probability distributions for the six parameters in question. In practice, information about $\pi(\mathcal{K})$ is available via a large number of samples $\mathcal{K}_i$ whose distribution matches $\pi(\mathcal{K})$.

Given the uncertainty in the reaction parameters $\mathcal{K}$, we should replace the objective function $C(\theta, \mathcal{K})$ in (10) by the statistical expectation value

$$\begin{aligned} C_{\text{stochastic}}(\theta) &= \mathbb{E}_{\pi(\mathcal{K})}[C_{\text{deterministic}}(\theta, \mathcal{K})] \\ &= \mathbb{E}_{\pi(\mathcal{K})}[w_1|\mu(\theta, \mathcal{K}) - \hat{\mu}| + w_2\sigma(\theta, \mathcal{K}) \\ &\quad + w_3 I_{\text{conversion}}(\theta, \mathcal{K})] \\ &= w_1\mathbb{E}_{\pi(\mathcal{K})}[|\mu(\theta, \mathcal{K}) - \hat{\mu}|] \\ &\quad + w_2\mathbb{E}_{\pi(\mathcal{K})}[\sigma(\theta, \mathcal{K})] \\ &\quad + w_3\mathbb{E}_{\pi(\mathcal{K})}[I_{\text{conversion}}(\theta, \mathcal{K})] \end{aligned} \tag{12}$$

In these expressions, $\mathbb{E}_{\pi(\mathcal{K})}$ denotes the expectation value defined for any function $f(\mathcal{K})$ by

$$\mathbb{E}_{\pi(\mathcal{K})}[f] = \int f(\mathcal{K})\pi(\mathcal{K})\mathrm{d}\mathcal{K} \tag{13}$$

Because $\pi(\mathcal{K})$ is only known through samples, we approximate the expectation values above[a] with Monte Carlo integration[57] via the formula

$$\mathbb{E}_{\pi(\mathcal{K})}[f] \approx \frac{1}{N}\sum_{i=1}^{N} f(\mathcal{K}_i) \tag{14}$$

where as mentioned, $\mathcal{K}_i$ is a set of N samples that are distributed proportional to $\pi(\mathcal{K})$. That is, we will choose a sufficiently large number N of samples and then optimize an approximate cost function based on that defined in (12)

$$\tilde{C}_{\text{stochastic}}(\theta) = \frac{1}{N}\sum_{i=1}^{N} C_{\text{deterministic}}(\theta, \mathcal{K}_i) \tag{15}$$

In this context, our goal has now changed to the following optimization under uncertainty problem: Find that set of control variables $\theta^*_{\text{stochastic}}$ that minimizes $\tilde{C}_{\text{stochastic}}(\theta)$. In other words, we seek to solve the following problem: Find θ^* so that

$$\theta^*_{\text{stochastic}} = \arg\min_{\theta} \tilde{C}_{\text{stochastic}}(\theta) \tag{16}$$

3.4. Remark 1. Problem (16) minimizes $\tilde{C}_{\text{stochastic}}(\theta)$ defined in (15), that is, we seek to find the minimum of the average of the objective functions $C_{\text{deterministic}}(\theta, \mathcal{K}_i)$ over the samples $\mathcal{K}_i$. This is often appropriate, but because we do not know which of the $\mathcal{K}_i$ is the "true" set of reaction parameters, it is also conceivable that $\theta^*_{\text{stochastic}}$ is a poor choice.[b] This is frequently addressed by adding "risk" terms in the definition of $C_{\text{stochastic}}$ in (15), see for example ref 31. We have experimented with this but found it unnecessary for the work presented here.

3.5. Optimization Algorithm. Equation 16 defines the optimization problem under uncertainty we would like to solve: Namely, to find those experimental conditions ("inputs") θ that minimize the stochastic cost function (i.e., how close the expected "outputs" are to desired values). In this section, let us discuss the algorithm that finds this minimizer.

Two key observations about the objective function $\tilde{C}_{\text{stochastic}}(\theta)$ will drive our choice of algorithm: (i) It is an expensive function to compute because every evaluation requires the solution of N forward solves of the ODEs that describe the progression of the reactions [i.e., the "forward model" (6)] for each of the samples $\mathcal{K}_i$ we use to represent the uncertainty in our knowledge of reaction rates. (ii) It is not practically feasible to compute derivatives of $\tilde{C}_{\text{stochastic}}(\theta)$ with regard to the experimental conditions encoded in θ. As a consequence, we need an algorithm for finding the minimum of $\tilde{C}_{\text{stochastic}}(\theta)$ that is both efficient in how many function evaluations it requires, and that is "derivative-free". In this work, we use the "Bayesian optimization"[c] framework built into the Matlab Statistics and Machine Learning Toolbox.[58] The reader can find alternative implementations in, for example, Python[59,60] and C++[61] depending on their software needs.

Bayesian optimization algorithms[62−64] for finding the minimizer of a function such as $\tilde{C}_{\text{stochastic}}(\theta)$ evaluate the objective function at a number of points and then ask (i) where

https://doi.org/10.1021/acsanm.4c01373
ACS Appl. Nano Mater. 2024, 7, 14090−14101

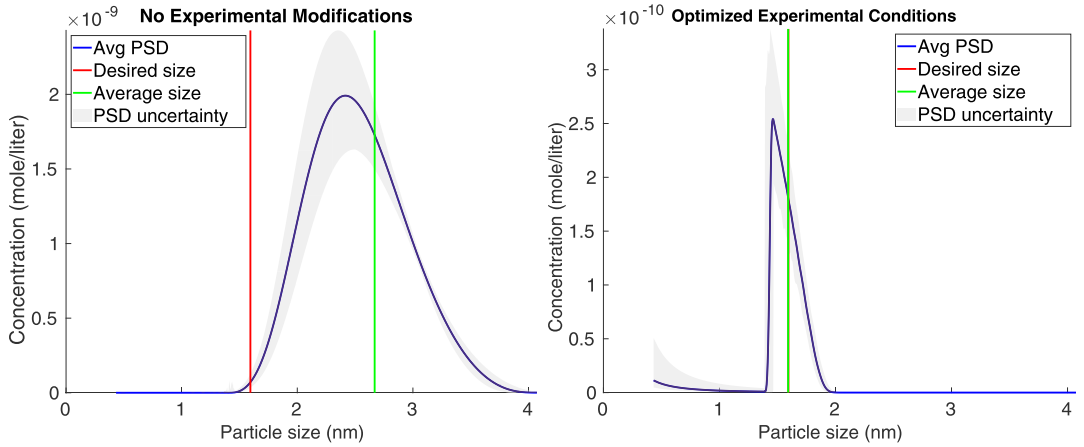

Figure 3. (Left) Predicted PSD (in blue) corresponding to the original particle synthesis experiment described in ref 39. (right) Predicted PSD (in blue) that results from optimization when only the experimental conditions are subject to variation. The gray shading indicates the uncertainty in the PSD due to the fact that we do not actually know reaction parameters exactly, but only their probability distribution $\pi(\mathcal{K})$, see Section 2. The blue line shows the statistical mean of the gray-shaded area for each PS.

in θ space the minimizer likely is, given the knowledge so far accumulated about $\tilde{C}_{\text{stochastic}}(\theta)$, and (ii) which parts of θ space have so far been poorly explored and may hold the minimizer. In other words, the algorithm balances the inefficiency of carefully exploring the parameter space against the efficiency of only looking in the most obvious places. The end result after evaluating $\tilde{C}_{\text{stochastic}}(\theta)$ at a number of locations θ_k is an approximation $\tilde{\theta}^*_{\text{stochastic}}$ – typically quite close—of the true minimizer $\theta^*_{\text{stochastic}}$, along with a certificate of how likely it is that there are no better minimizers anywhere else in θ space. The more function evaluations we are willing to allow, the better the approximation $\tilde{\theta}^*_{\text{stochastic}}$ of $\theta^*_{\text{stochastic}}$, and the firmer the certificate.

We have found the algorithm described above to be very efficient in approximating $\theta^*_{\text{stochastic}}$. It is conceivable that specialized algorithms for optimization under uncertainty—such as variants of the stochastic gradient method[65−68]—could reduce the computational cost further, provided one can compute a gradient. Indeed, with substantial effort, one could also implement methods that compute derivatives of $\tilde{C}_{\text{stochastic}}(\theta)$ after all,[69] generating information necessary for derivative-based optimization algorithms. In the end, we have found the computational cost of Bayesian optimization acceptable, and the effort of implementing different methods is not necessary to obtain the results we will show in the following section.

4. RESULTS

Having described in the previous section how we define optimal outcomes and how we algorithmically find optimal inputs, let us in the following show what these methods yield. As mentioned in the introduction, the main goal of our study is to determine whether the mathematical model we use for the nucleation and growth of iridium nanoparticles allows for control over both the size and the size distribution of particles; as we will illustrate below, the answer to this question is "yes".

For the experiments we present below, we need to select weights w_i in our cost function (12). Recall that w_1 weights the importance of the mean particle value matching the desired PS, w_2 weights the importance of having a narrow PSD, and w_3 weights the importance of consuming all of the precursor species in the reaction. Our choice is heuristic, taking into account that the resulting weighted terms in (12) need to have the same physical units. In particular, we choose the w_i so that each term in the objective function (12) scales to approximately a unit value for a "poor" result. First, we notice that, for the typical experimental conditions under which our iridium particles are created, the particles sizes are roughly 2−3 nm and hence creating particles 1 nm different than $\hat{\mu}$ would be considered a poor result. Thus, we choose $w_1 = 5$. We desire a PSD that is narrower than the baseline of ref 39 (shown in the left panel of Figure 3) but do not consider this a poor result; this baseline has a PSD with a standard deviation $\sigma = 4.3 \times 10^{-1}$ nm. So we choose $w_2 = 1$ since we consider having a spread twice as wide—and hence $\sigma \approx 1$ nm—would certainly be a poor result. Finally, we choose $w_3 = 5$ so a reaction utilizing 20% of the precursor species would be considered as bad as a reaction producing a mean PS 0.2 nm from $\hat{\mu}$. In summary, the weights in (10) that we use for our explorations below are $w_1 = 5$, $w_2 = 1$, $w_3 = 5$.

4.1. Experiment 1: Optimizing Experimental Conditions. In the first experiment, we consider optimization of $\tilde{C}_{\text{stochastic}}(\theta)$ where $\theta = \{t_{\text{end}}, A_0, \text{POM}_0\}$ consists of those variables that are experimentally easily accessible: namely, the end time t_{end} at which we quench the reaction, the initial precursor concentration A_0, and the initial POM concentration POM_0. We recall that for the experiments reported in ref 39—which we used to determine the reaction parameters $\mathcal{K}$, see Table 1 and ref 31—we had used $t_{\text{end}} = 4.838$ h, $A_0 = 1.2 \times 10^{-3}$ molL^{-1}, $\text{POM}_0 = 0$ mol L^{-1}. These values resulted in a mean PS of $\mu = 2.67$ nm and a standard deviation of $\sigma = 4.3 \times 10^{-1}$ nm.

Let us target a mean PS of $\hat{\mu} = 1.59$ (corresponding to 150 iridium atoms). Utilizing the objective function defined in (15), the weights discussed in the introduction to this section, and the algorithm described in Section 3.4, we obtain an optimal PSD as shown in the right panel of Figure 3.

The optimal experimental conditions that resulted in the distribution shown in the figure are $\theta^*_{\text{stochastic}} = \{t_{\text{end}} = 2.815$ h, $A_0 = 1.018 \times 10^{-4}$ mol L^{-1}, $\text{POM}_0 = 1.0015 \times 10^{-4}$ mol L$^{-1}\}$. It is clear from the figure that the optimization has achieved its goal: Not only is the mean PS $\mu = 1.59$ nm (indicated by the green line) nearly indistinguishable from the desired one $\hat{\mu}$ (indicated by the red line), but particles also occupy only a fairly narrow size range, between approximately 1.5 and 2 nm; the standard

https://doi.org/10.1021/acsanm.4c01373
ACS Appl. Nano Mater. 2024, 7, 14090−14101

deviation for the PS is $\sigma = 1.4 \times 10^{-1}$ nm, substantially less than the baseline results.

At the same time, the reaction conditions chosen by the algorithm lead to a fairly short reaction time at the end of which only a relatively small fraction (16.9%) of the precursor has been converted into nanoparticles—in other words, we quench the reaction prematurely to avoid particles growing larger than desired. As a consequence, the concentrations of particles of various sizes shown in Figure 3 are quite small, on the order of 10^{-10} mol/liter for each PS separately. The remaining fraction of (unused) iridium, defined in (9), is $I_{\text{conversion}} = 0.83$.

4.2. Experiment 2: Optimizing Experimental Conditions and Reaction Factors. The results of the previous section indicate that one can indeed optimize both the mean PS, and the dispersion of PSs, using only the experimental conditions. Yet, variations of the iridium system we consider here may also be amenable to making other parameters accessible to optimization—see the discussion in Section 3.1. Specifically, we repeat the experiments of the previous subsection but consider $\theta = \{t_{\text{end}}, A_0, \text{POM}_0, \alpha_{kf}, \alpha_{k1}\}$ where α_{kf} and α_{k1} are multipliers for the k_f reaction rate and the k_1 reaction rates, respectively.

Using this expanded set of optimization variables, and using the same values for $\hat{\mu}$ and the weighting factors as in the previous subsection, we obtain an optimal PSD as shown in Figure 4.

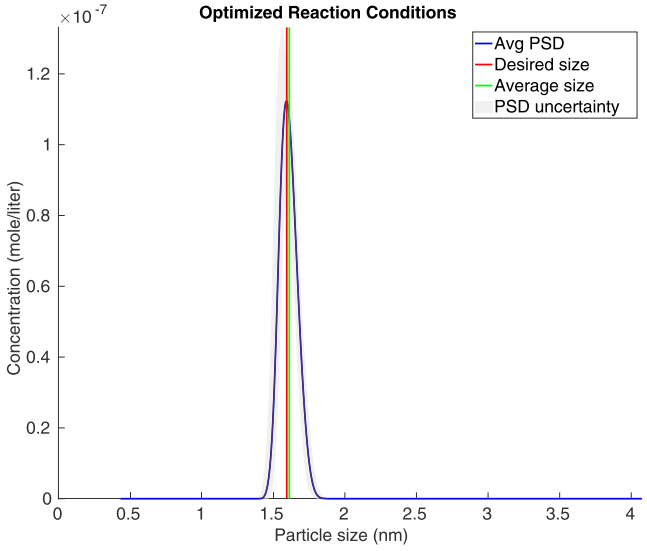

Figure 4. Optimal PSD when optimizing the experimental conditions t_{end}, A_0, POM_0, along with the multipliers α_{kf} and α_{k1}. This optimization result consists of a mean PS 1% off of the desired size, ≥95% of the particles within ±10% of the mean size (i.e., near-monodisperse), and utilizing the precursor efficiently by converting more than 99.9% of the iridium to particles.

Comparing this figure with that in Figure 3, it is clear that the optimization algorithm is able to further minimize the dispersion of PSs—nearly all particles are now within just 10% of the mean PS—while maintaining an excellent match to the intended PS. Numerically, the mean PS is now $\mu = 1.6$ nm—only 1% larger than the desired size—with a standard deviation of $\sigma = 6 \times 10^{-2}$ nm; that is, a a very narrow PSD of only ±3.8% (any PSD under 5% being in record territory as discussed in ref 70 on page 6557). Furthermore, the reaction leads to 1000 times higher concentrations, with concentrations on the order of 10^{-7} mol L^{-1}. Finally, the overall conversion inefficiency, defined in (9), has now been reduced to $I_{\text{conversion}} = 6 \times 10^{-5}$. The experimental conditions and multipliers that produce this outcome are $\theta^*_{\text{stochastic}} = \{t_{\text{end}} = 4.04\text{ h}, A_0 = 7.9 \times 10^{-4}\text{ mol L}^{-1}, \text{POM}_0 = 1 \times 10^{-4}\text{ mol L}^{-1}, \alpha_{kf} = 9.96, \alpha_{k1} = 9.65\}$. Hence, additionally allowing the reaction conditions to be modified through means to the conditions listed just above will allow for much more precise control over the PSD, with our optimization achieving a near-perfect match to the desired PS, a low-dispersion PSD, and an efficient experiment in that the reaction is run to completion.

5. CONCLUSIONS

Herein, we have shown that it is possible to optimize the size and size distribution of nanoparticles given a mechanistic model for particle formation along with estimates of the reaction rates in the model. As we have shown, we can then formulate an optimization problem and solve it with appropriate algorithms, the results of which produce predictions of PSs that are not only close to desired values but also narrowly distributed around that desired value. In other words, our results show that for the system of iridium particles we consider here, it is possible not only to control the PS, but also the dispersion of sizes: That is, we can aspire to use these methods to tailor reaction outcomes to very specific tasks for which nanoparticles are uniquely suited!

In summary, we have (i) provided an easy-to-implement approach to optimization of a nanoparticle synthesis and PSD, (ii) constructed and posted on GitHub the necessary code along with instructions to install and reproduce our computational results (see https://github.com/dklong-csu/mepbm), and thereby (iii) demonstrated proof-of-principle optimization under uncertainty of a nanoparticle synthesis, whose mathematical methodology is sufficiently general to be applicable also to other particle syntheses. Our approach is general to nano- and larger particles by building on a flexible framework for modeling the concentrations of particles of different sizes, accounting for statistical noise in the data and mathematical model (Bayesian inversion), incorporating parameter probability distributions in the optimization problem (optimization under uncertainty), and utilizing an accessible global optimization algorithm to efficiently determine the best experimental design for one's desired outcome (Bayesian optimization). Hence, it is reasonable to anticipate the optimization workflow we presented in this work to be of great value in optimizing the synthesis of other particle systems and for experimental checks to validate our predicted synthesis.

The work we have presented here clearly points to a number of avenues for future research:

- For the iridium particles we used as a proof-of-principle, we have identified experimental conditions for which the model predicts PSDs that are substantially narrower, as well as much better centered around a desired size, than the ones we have obtained in previous experiments. A clear goal for future work would be to experimentally validate these predictions. It is clear that such an experimental validation would have made the current study far more convincing; unfortunately, despite our past work in this area, this validation is no longer within the experimental abilities of the authors' laboratories.
- As mentioned before, we have used the iridium nanoparticle system used herein primarily because of its excellent characterization. Yet, the optimization approach of Section 3 is not specific to the iridium system, nor indeed to the use of models such as the one we have

https://doi.org/10.1021/acsanm.4c01373
ACS Appl. Nano Mater. 2024, 7, 14090−14101

outlined in Section 2. Given a sufficient faithful model of particle formation, the methods we have described herein can and should also be applied to other systems.

- In order to address real-world syntheses, optimization methods need to take constraints on optimization as well as state variables into account. These include physical limitations on initial concentrations that are experimentally accessible, limits on temperature ranges, and safety and cost considerations. We have ignored these for the purposes of this study, although they are readily included in the application of the algorithms we have presented. In practice, most of these constraints are simply lower and upper bounds on specific optimization variables that are easily incorporated in the formulations of Sections 3.3 and 3.4, as well as into the algorithms we have used to perform the actual optimization.

It would also be worthwhile incorporating cost considerations—not just desirable physical and chemical properties—into the objective function. For example, today's nanoparticle syntheses cannot create the narrow size distributions required for applications, and consequently often need to be microfiltered at high cost and resultant low yield. In such cases, optimizing PSs does not only result in more desirable sizes but also results in cost savings.

- More broadly, our methods to predict optimized conditions of particle syntheses for a broad class of particles provide an experimentalist not only with synthesis conditions that produce a desired outcome. Rather, these are also appropriate experimental conditions to learn more about the particle formation mechanisms and that allow, should experimental outcomes not faithfully match computational predictions, for the efficient refinement of the underlying mathematical model.

AUTHOR INFORMATION

Corresponding Author

Danny Long − *Department of Mathematics, Colorado State University, Fort Collins, Colorado 80523, United States; Institute of Particle Technology, Friedrich-Alexander University Erlangen-Nürnberg, Erlangen 91058, Germany;* orcid.org/0000-0002-5812-2364; Email: dannylongcsu@gmail.com

Authors

Richard G. Finke − *Department of Chemistry, Colorado State University, Fort Collins, Colorado 80523, United States*

Wolfgang Bangerth − *Department of Mathematics, Colorado State University, Fort Collins, Colorado 80523, United States; Department of Geosciences, Colorado State University, Fort Collins, Colorado 80523, United States;* orcid.org/0000-0003-2311-9402

Complete contact information is available at: https://pubs.acs.org/10.1021/acsanm.4c01373

Notes

The authors declare no competing financial interest.

ACKNOWLEDGMENTS

DKL's research time was supported by the U.S. Department of Energy, Office of Science, Basic Energy Sciences, Catalysis Science Program, via Award SE-FG402-02ER15453 to RFG, by the National Science Foundation award DMS-1821210, and by the Deutsche Forschungsgemeinschaft (DFG, German Research Foundation)—project-ID 416229255—SFB 1411. RGF's time was supported by National Science Foundation grant no. 1664646. WB's research was partially supported by the National Science Foundation under award OAC-1835673 as part of the Cyberinfrastructure for Sustained Scientific Innovation (CSSI) program; by award DMS-1821210; by award EAR-1925595.

ADDITIONAL NOTES

[a] Alternative methods for approximating the integral in (13′) are possible and can equivalently be used in our framework. For example, when the forward model f is computationally demanding, one could use Polynomial Chaos Expansions.[54] One can compute these in a black-box manner in a number of software packages, for example, in Matlab,[46,55] Python,[47,56] and C++.[47]

[b] Perhaps a better description of the issue would be to say that if one were to perform more experiments, one might obtain a different—and hopefully more localized—probability distribution $\hat{\pi}(\mathcal{K})$. In that case, the optimal parameter $\theta^*_{\text{stochastic}}$ found for $\pi(\mathcal{K})$ may not have been a great choice for $\hat{\pi}(\mathcal{K})$.

[c] The term "Bayesian optimization" describes a set of methods that take into account how much we believe we know about the objective function at a point θ, having previously evaluated the objective function at a set of other points. Except for the fact that it incorporates "uncertainty" into the optimization process, "Bayesian optimization" is unrelated to the "Bayesian inverse problem" we have used to assess how much we know about the reaction parameters $\mathcal{K}$ in Section 2.

REFERENCES

(1) Reiss, H. The Growth of Uniform Colloidal Dispersions. *J. Chem. Phys.* **1951**, *19*, 482−487.

(2) Krishna, P. H.; Ramrakhiani, M. Effect of particle size distribution on spectral characteristics of different quantum dots. *Int. J. Appl. Eng. Res.* **2018**, *13*, 1722−1727.

(3) Stöber, W.; Fink, A.; Bohn, E. Controlled growth of monodisperse silica spheres in the micron size range. *J. Colloid Interface Sci.* **1968**, *26*, 62−69.

(4) Matijevic, E. Preparation and properties of uniform size colloids. *Chem. Mater.* **1993**, *5*, 412−426.

(5) Chen, H.; Shao, L.; Li, Q.; Wang, J. Gold nanorods and their plasmonic properties. *Chem. Soc. Rev.* **2013**, *42*, 2679−2724.

(6) Gilroy, K. D.; Ruditskiy, A.; Peng, H.-C.; Qin, D.; Xia, Y. Bimetallic Nanocrystals: Syntheses, Properties, and Applications. *Chem. Rev.* **2016**, *116*, 10414−10472.

(7) Cortie, M. B.; McDonagh, A. M. Synthesis and Optical Properties of Hybrid and Alloy Plasmonic Nanoparticles. *Chem. Rev.* **2011**, *111*, 3713−3735.

(8) An, L.; Wang, Y.; Tian, Q.; Yang, S. Small Gold Nanorods: Recent Advances in Synthesis, Biological Imaging, and Cancer Therapy. *Materials* **2017**, *10*, 1372.

(9) Khan, I.; Saeed, K.; Khan, I. Nanoparticles: Properties, applications and toxicities. *Arab. J. Chem.* **2019**, *12*, 908−931.

(10) Tsui, K.-L. An overview of Taguchi method and newly developed statistical methods for robust design. *IIE Trans.* **1992**, *24*, 44−57.

(11) Boudart, M. Catalysis by Supported Metals. *Adv. Catal.* **1969**, *20*, 153−166.

(12) Bond, G. C. Strategy of research on supported metal catalysts. Problems of structure-sensitive reactions in the gas phase. *Acc. Chem. Res.* **1993**, *26*, 490−495.

(13) Suresh, S. Semiconductor nanomaterials, methods and applications: A review. *Nanosci. Nanotechnol.* **2013**, *3*, 62−74.

(14) Jang, E.; Jang, H. Review: Quantum Dot Light-Emitting Diodes. *Chem. Rev.* **2023**, *123*, 4663−4692.
(15) Sadeghi, S.; Abkenar, S. K.; Ow-Yang, C. W.; Nizamoglu, S. Efficient White LEDs Using Liquid-state Magic-sized CdSe Quantum Dots. *Sci. Rep.* **2019**, *9*, 10061−10069.
(16) Park, J.; Lee, J. H.; Doh, H.; Heo, S. W.; Cho, K.; Kim, S.; Cho, S.; Bang, J. Size-Dependent Photovoltaic Performance of CdSe Supra-quantum Dot/Polymer Hybrid Solar Cells: "Goldilocks Problem" Resolved by Tuning the Band Alignment Using Surface Ligands. *J. Phys. Chem. C* **2020**, *124*, 25775−25783.
(17) He, T.; Chen, D.; Jiao, X.; Wang, Y.; Duan, Y. Solubility-Controlled Synthesis of High-Quality Co3O4 Nanocrystals. *Chem. Mater.* **2005**, *17*, 4023−4030.
(18) Yang, S.; Liu, Q. Formation mechanism of apex-truncated octahedral Cu2O microcrystal. *CrystEngComm* **2016**, *18*, 8229−8236.
(19) Stolzenburg, P.; Garnweitner, G. Experimental and numerical insights into the formation of zirconia nanoparticles: a population balance model for the nonaqueous synthesis. *React. Chem. Eng.* **2017**, *2*, 337−348.
(20) Ng, J.; Xu, S.; Zhang, X.; Yang, H. Y.; Sun, D. D. Hybridized Nanowires and Cubes: A Novel Architecture of a Heterojunctioned TiO2/SrTiO3 Thin Film for Efficient Water Splitting. *Adv. Funct. Mater.* **2010**, *20*, 4287−4294.
(21) Mehranpour, H.; Askari, M.; Ghamsari, M. S.; Farzalibeik, H. Study on the Phase Transformation Kinetics of Sol-Gel Drived TiO2 Nanoparticles. *J. Nanomater.* **2010**, *2010*, 1−5.
(22) Bailey, J. K.; Brinker, C.; Mecartney, M. L. Growth Mechanisms of Iron Oxide Particles of Differing Morphologies from the Forced Hydrolysis of Ferric Chloride Solutions. *J. Colloid Interface Sci.* **1993**, *157*, 1−13.
(23) Kwon, S. G.; Piao, Y.; Park, J.; Angappane, S.; Jo, Y.; Hwang, N.-M.; Park, J.-G.; Hyeon, T. Kinetics of Monodisperse Iron Oxide Nanocrystal Formation by "Heating-Up" Process. *J. Am. Chem. Soc.* **2007**, *129*, 12571−12584.
(24) Lassenberger, A.; Grünewald, T. A.; van Oostrum, P. D. J.; Rennhofer, H.; Amenitsch, H.; Zirbs, R.; Lichtenegger, H. C.; Reimhult, E. Monodisperse Iron Oxide Nanoparticles by Thermal Decomposition: Elucidating Particle Formation by Second-Resolved in Situ Small-Angle X-ray Scattering. *Chem. Mater.* **2017**, *29*, 4511−4522.
(25) Dehsari, H. S.; Harris, R. A.; Ribeiro, A. H.; Tremel, W.; Asadi, K. Optimizing the Binding Energy of the Surfactant to Iron Oxide Yields Truly Monodisperse Nanoparticles. *Langmuir* **2018**, *34*, 6582−6590.
(26) Korevaar, P. A.; de Greef, T. F. A.; Meijer, E. W. Pathway Complexity in π-Conjugated Materials. *Chem. Mater.* **2014**, *26*, 576−586.
(27) Zhang, R.; Khalizov, A.; Wang, L.; Hu, M.; Xu, W. Nucleation and Growth of Nanoparticles in the Atmosphere. *Chem. Rev.* **2012**, *112*, 1957−2011.
(28) Handwerk, D. R.; Shipman, P. D.; Whitehead, C. B.; Özkar, S.; Finke, R. G. Mechanism-Enabled Population Balance Modeling of Particle Formation en Route to Particle Average Size and Size Distribution Understanding and Control. *J. Am. Chem. Soc.* **2019**, *141*, 15827−15839.
(29) Handwerk, D. R.; Shipman, P. D.; Whitehead, C. B.; Özkar, S.; Finke, R. G. Particle Size Distributions via Mechanism-Enabled Population Balance Modeling. *J. Phys. Chem. C* **2020**, *124*, 4852−4880.
(30) Long, D. K.; Bangerth, W.; Handwerk, D. R.; Whitehead, C. B.; Shipman, P. D.; Finke, R. G. Estimating reaction parameters in mechanism-enabled population balance models of nanoparticle size distributions: A Bayesian inverse problem approach. *J. Comput. Chem.* **2022**, *43*, 43−56.
(31) Long, D. Quantification and Application of Uncertainty in the Formation of Nanoparticles. Ph.D. thesis; Colorado State University, 2023.
(32) Hulburt, H.; Katz, S. Some problems in particle technology. *Chem. Eng. Sci.* **1964**, *19*, 555−574.
(33) McGraw, R. Description of Aerosol Dynamics by the Quadrature Method of Moments. *Aerosol Sci. Technol.* **1997**, *27*, 255−265.
(34) Li, D.; Li, Z.; Gao, Z. Quadrature-based moment methods for the population balance equation: An algorithm review. *Chin. J. Chem. Eng.* **2019**, *27*, 483−500.
(35) Pflug, L.; Schikarski, T.; Keimer, A.; Peukert, W.; Stingl, M. eMoM Exact method of moments—Nucleation and size dependent growth of nanoparticles. *Comput. Chem. Eng.* **2020**, *136*, 106775.
(36) Dienstbier, J.; Aigner, K.-M.; Rolfes, J.; Peukert, W.; Segets, D.; Pflug, L.; Liers, F. Robust optimization in nanoparticle technology: A proof of principle by quantum dot growth in a residence time reactor. *Comput. Chem. Eng.* **2022**, *157*, 107618.
(37) Lin, Y.; Finke, R. G. Novel Polyoxoanion- and Bu4N+-Stabilized, Isolable, and Redissolvable, 20−30-.ANG. Ir300−900 Nanoclusters: The Kinetically Controlled Synthesis, Characterization, and Mechanism of Formation of Organic Solvent-Soluble, Reproducible Size, and Reproducible Catalytic Activity Metal Nanoclusters. *J. Am. Chem. Soc.* **1994**, *116*, 8335−8353.
(38) Lin, Y.; Finke, R. G. A More General Approach to Distinguishing "Homogeneous" from "Heterogeneous" Catalysis: Discovery of Polyoxoanion- and Bu4N+-Stabilized, Isolable and Redissolvable, High-Reactivity Ir.apprx.190−450 Nanocluster Catalysts. *Inorg. Chem.* **1994**, *33*, 4891−4910.
(39) Watzky, M. A.; Finney, E. E.; Finke, R. G. Transition-Metal Nanocluster Size vs Formation Time and the Catalytically Effective Nucleus Number: A Mechanism-Based Treatment. *J. Am. Chem. Soc.* **2008**, *130*, 11959−11969.
(40) Watzky, M. A.; Finke, R. G. Pseudoelementary Steps: A Key Concept and Tool for Studying the Kinetics and Mechanisms of Complex Chemical Systems. *J. Phys. Chem. A* **2021**, *125*, 10687−10705.
(41) Schmidt, A.; Smirnov, V. Concept of "magic" number clusters as a new approach to the interpretation of unusual kinetics of the Heck reaction with aryl bromides. *Top. Catal.* **2005**, *32*, 71−75.
(42) Smith, R. C. *Uncertainty Quantification: Theory, Implementation, and Applications*; Society for Industrial and Applied Mathematics, 2014.
(43) van Ravenzwaaij, D.; Cassey, P.; Brown, S. D. A simple introduction to Markov Chain Monte−Carlo sampling. *Psychon. Bull. Rev.* **2018**, *25*, 143−154.
(44) Foreman-Mackey, D.; Hogg, D. W.; Lang, D.; Goodman, J. emcee: The MCMC Hammer. *Publ. Astron. Soc. Pac.* **2013**, *125*, 306−312.
(45) Wagner, P.-R.; Nagel, J.; Marelli, S.; Sudret, B. *UQLab User Manual—Bayesian Inversion for Model Calibration and Validation; Report UQLab-V2.0-113*, 2022.
(46) Marelli, S.; Sudret, B. *UQLab: A Framework for Uncertainty Quantification in Matlab. Vulnerability, Uncertainty, and Risk*, 2014.
(47) Parno, M.; Davis, A.; Seelinger, L. MUQ: The MIT Uncertainty Quantification Library. *J. Open Source Softw.* **2021**, *6*, 3076.
(48) Taylor, C. J.; Pomberger, A.; Felton, K. C.; Grainger, R.; Barecka, M.; Chamberlain, T. W.; Bourne, R. A.; Johnson, C. N.; Lapkin, A. A. A Brief Introduction to Chemical Reaction Optimization. *Chem. Rev.* **2023**, *123*, 3089−3126.
(49) Rezaeianjouybari, B.; Sheikholeslami, M.; Shafee, A.; Babazadeh, H. A novel Bayesian optimization for flow condensation enhancement using nanorefrigerant: A combined analytical and experimental study. *Chem. Eng. Sci.* **2020**, *215*, 115465.
(50) Hickman, R. J.; Aldeghi, M.; Häse, F.; Aspuru-Guzik, A. Bayesian optimization with known experimental and design constraints for chemistry applications. *Digital Discovery* **2022**, *1*, 732−744.
(51) Tao, H.; Wu, T.; Aldeghi, M.; Wu, T. C.; Aspuru-Guzik, A.; Kumacheva, E. Nanoparticle synthesis assisted by machine learning. *Nat. Rev. Mater.* **2021**, *6*, 701−716.
(52) Mekki-Berrada, F.; Ren, Z.; Huang, T.; Wong, W. K.; Zheng, F.; Xie, J.; Tian, I. P. S.; Jayavelu, S.; Mahfoud, Z.; Bash, D.; Hippalgaonkar, K.; Khan, S.; Buonassisi, T.; Li, Q.; Wang, X. Two-step machine learning enables optimized nanoparticle synthesis. *npj Comput. Mater.* **2021**, *7*, 55.
(53) Ott, L. S.; Finke, R. G. Transition-metal nanocluster stabilization for catalysis: A critical review of ranking methods and putative stabilizers. *Coord. Chem. Rev.* **2007**, *251*, 1075−1100.

https://doi.org/10.1021/acsanm.4c01373
ACS Appl. Nano Mater. 2024, 7, 14090−14101

(54) Lüthen, N.; Marelli, S.; Sudret, B. Sparse Polynomial Chaos Expansions: Literature Survey and Benchmark. *SIAM/ASA J. Uncertain. Quantification* **2021**, *9*, 593−649.
(55) Marelli, S.; Lüthen, N.; Sudret, B. *UQLab User Manual—Polynomial Chaos Expansions; Report UQLab-V2.0-104*, 2022.
(56) Olivier, A.; Giovanis, D. G.; Aakash, B.; Chauhan, M.; Vandanapu, L.; Shields, M. D. UQpy: A general purpose Python package and development environment for uncertainty quantification. *J. Comput. Sci.* **2020**, *47*, 101204.
(57) Caflisch, R. E. Monte Carlo and quasi-Monte Carlo methods. *Acta Numer.* **1998**, *7*, 1−49.
(58) The MathWorks, Inc. *Statistics and Machine Learning Toolbox*; The MathWorks, Inc., 2023.
(59) Klein, A.; Falkner, S.; Mansur, N.; Hutter, F. RoBO: A Flexible and Robust Bayesian Optimization Framework in Python. *NIPS 2017 Bayesian Optimization Workshop*; NIPS, 2017.
(60) Nogueira, F. Bayesian Optimization: Open source constrained global optimization tool for Python, 2014. https://github.com/fmfn/BayesianOptimization. Accessed Date September 1, 2023.
(61) Cully, A.; Chatzilygeroudis, K.; Allocati, F.; Mouret, J.-B. Limbo A Flexible High-performance Library for Gaussian Processes modeling and Data-Efficient Optimization. *J. Open Source Softw.* **2018**, *3*, 545.
(62) Kushner, H. J. A versatile stochastic model of a function of unknown and time varying form. *J. Math. Anal. Appl.* **1962**, *5*, 150−167.
(63) Garnett, R. *Bayesian Optimization*; Cambridge University Press, 2023.
(64) Rasmussen, C. E.; Williams, C. K. I. *Gaussian Processes for Machine Learning*; The MIT Press, 2005.
(65) Robbins, H.; Monro, S. A Stochastic Approximation Method. *Ann. Math. Stat.* **1951**, *22*, 400−407.
(66) Schmidt, M.; Le Roux, N.; Bach, F. Minimizing finite sums with the stochastic average gradient. *Math. Program.* **2016**, *162*, 83−112.
(67) Bottou, L.; Curtis, F. E.; Nocedal, J. Optimization Methods for Large-Scale Machine Learning. *SIAM Rev.* **2018**, *60*, 223−311.
(68) Pflug, L.; Bernhardt, N.; Grieshammer, M.; Stingl, M. CSG: A new stochastic gradient method for the efficient solution of structural optimization problems with infinitely many states. *Struct. Multidiscip. Optim.* **2020**, *61*, 2595−2611.
(69) Tortorelli, D. A.; Michaleris, P. Design sensitivity analysis: Overview and review. *Inverse Probl. Eng.* **1994**, *1*, 71−105.
(70) Özkar, S.; Finke, R. G. Dust Effects on Nucleation Kinetics and Nanoparticle Product Size Distributions: Illustrative Case Study of a Prototype $Ir(0)_n$ Transition-Metal Nanoparticle Formation System. *Langmuir* **2017**, *33*, 6550−6562.

https://doi.org/10.1021/acsanm.4c01373
ACS Appl. Nano Mater. 2024, 7, 14090−14101